Lunar active seismic profiler for investigating shallow substrates of the Moon and other extraterrestrial environments

Takeshi Tsuji, Taizo Kobayashi, Junji Kinoshita, Tatsunori Ikeda, Tomoki Uchigaki, Yuichiro Nagata, Taichi Kawamura, Kazunori Ogawa, Satoshi Tanaka, Akito Araya

Icarus 404 (2023) 115666

Contents lists available at ScienceDirect

Icarus

journal homepage: www.elsevier.com/locate/icarus

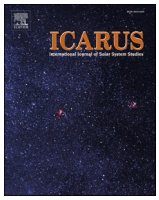

Lunar active seismic profiler for investigating shallow substrates of the Moon and other extraterrestrial environments

Takeshi Tsuji [a,*], Taizo Kobayashi [b], Junji Kinoshita [c], Tatsunori Ikeda [c], Tomoki Uchigaki [c], Yuichiro Nagata [c], Taichi Kawamura [d], Kazunori Ogawa [e], Satoshi Tanaka [e], Akito Araya [f]

[a] School of Engineering, The University of Tokyo, Tokyo, Japan
[b] Department of Civil and Environmental Engineering, Ritsumeikan University, Shiga, Japan
[c] Graduate School of Engineering, Kyushu University, Fukuoka, Japan
[d] Université Paris Cité, Institut de physique du globe de Paris, CNRS, Paris, France
[e] Institute of Space and Astronautical Science (ISAS), Japan Aerospace Exploration Agency (JAXA), Kanagawa, Japan
[f] Earthquake Research Institute, The University of Tokyo, Tokyo, Japan

ARTICLE INFO

Keywords:
Moon, interior
Mars, interior
Instrumentation
Geophysics
Regoliths

ABSTRACT

To investigate the structures and properties of shallow material in extraterrestrial environments, we have developed a lunar active seismic profiler (LASP), which integrates active seismic sources and receivers in a short (~1 m) array that can be deployed on a rover. The small active source generates a chirp waveform that sweeps over a wide frequency range (20–250 Hz). The receivers are coupled to the ground by their own weight, but nevertheless deliver acceptable performance. We improve the signal-to-noise ratio of the seismic signal by stacking waveforms, enabling a minimal source to support the exploration of geological substrates. By processing shot gather of the LASP data, we calculated a dispersion curve of surface waves and obtained an accurate S-wave velocity profile from surface to 1 m depth. The results suggest that regions with even small amounts of subsurface ice (~0.5 wt%) can be identified in LASP results by their anomalously high S-wave velocity. Field experiments demonstrate that the LASP can support estimates of 3D S-wave velocity distributions and the identification of a buried geological boundary. The LASP also detected different degrees of compaction at the experimental site. If two rovers carry these profilers, or if a single rover combines one with a separately deployed receiver or active seismic source, seismic refraction and seismic reflection analyses can be conducted simultaneously in addition to surface wave analyses. These seismic surveys for longer-offset data achieve the exploration of deeper substrates in extraterrestrial settings such as the Moon, Mars, and other solid bodies.

1. Introduction

Seismic studies have yielded information about the interiors of planetary bodies that cannot be obtained in any other way. The Apollo missions deployed seismometers on the Moon and used them to investigate seismic events and geological substrates (Kovach et al., 1971, 1972; Coorper et al., 1974; Tanimoto et al., 2008; Heffels et al., 2017). Seismometers deployed on Mars have provided many geological observations and insights related to subsurface structures, seismic events, and ambient noise characteristics (Banerdt et al., 2020; Kenda et al., 2020; Knapmeyer-Endrun and Kawamura, 2020; Lognonné et al., 2020; Suemoto et al., 2020; Hobiger et al., 2021). However, the main objective of seismometer deployments on the Moon and Mars was to detect natural seismic events, and most of them relied on passive data. Seismic imaging based on passive data, whether seismic events or ambient noise, requires long observation times for data acquisition, which precludes making measurements at many locations, and the results are strongly dependent on the seismic or ambient noise characteristics of the site (Orita et al., 2021). On the other hand, active-source seismic surveys can obtain subsurface information in a short time and a well-controlled manner. In the Apollo missions, astronauts deployed active sources and successfully investigated the shallow substrate (Kovach et al., 1971,

* Corresponding author at: School of Engineering, The University of Tokyo, 7-3-1 Hongo, Bunkyo-ku, Tokyo 113-8656, Japan.
E-mail addresses: tsuji@sys.t.u-tokyo.ac.jp (T. Tsuji), kobat@fc.ritsumei.ac.jp (T. Kobayashi), kinoshita.junji.818@m.kyushu-u.ac.jp (J. Kinoshita), ikeda@mine.kyushu-u.ac.jp (T. Ikeda), uchigaki.tomoki.715@s.kyushu-u.ac.jp (T. Uchigaki), kawamura@ipgp.fr (T. Kawamura), ogawa.kazunori@jaxa.jp (K. Ogawa), tanaka@planeta.sci.isas.jaxa.jp (S. Tanaka), araya@eri.u-tokyo.ac.jp (A. Araya).

https://doi.org/10.1016/j.icarus.2023.115666
Received 19 February 2023; Received in revised form 2 June 2023; Accepted 2 June 2023
Available online 8 June 2023

1972; Coorper et al., 1974). More recently, an active seismic experiment using hammering was conducted on the Mars to investigate the regolith seismic velocity (Brinkman et al., 2022). As future space missions are conceived and developed, autonomous seismic surveys by rovers could be useful to explore extensive areas. A seismic exploration package compatible with small to middle-size spacecraft would therefore open a valuable avenue of investigation into the interiors of planetary bodies, including the Moon and Mars (Kawamura et al., 2022).

In an active-source seismic survey, the signals generated by a seismic source propagate through the ground and are received by multiple receivers (i.e., geophones and seismometers). Active-source data can support analytical methods based on different wave types, including surface wave analysis, seismic refraction analysis, and seismic reflection analysis. The optimum geometry of seismic sources and receivers is different for each method. The size and weight limits of spacecraft severely constrain the seismic equipment they can deliver. However, within these constraints, it is imperative to consider optimal seismic approaches to investigate subsurface structures.

To support seismic investigations of the lunar subsurface with portable equipment, we have designed and developed a Lunar Active Seismic Profiler (LASP) with multiple geophones and active sources (Tsuji et al., 2012a; Tsuji et al., 2019). The LASP was designed to investigate the shallow (<1 m) surface material of the Moon and Mars, mainly using surface wave information. The shallow target depth of our system allows the use of a short receiver array (~1 m). The shallow substrate is an important target because it may contain ice deposits that could be used as a resource. The seismic approach is useful for ice exploration because S-wave velocities in a porous medium vary with the degree of pore-fluid freezing (Zimmermann and King, 1986; see Appendix). Small amounts of frozen water in the voids of porous sediment or rock can lead to large increases in S-wave velocity (Johansen et al., 2003). Furthermore, the distribution of regolith and the depth to bedrock are critical information for constructing base camps. Measurements of regolith properties (e.g., degree of compaction) in situ are crucial for developing large human-occupied rovers as well as telescopes and other installations on the Moon (Tang et al., 2020). For these reasons, S-wave velocities derived from surface waves could be useful information for engineering and science on the Moon and Mars. Here we present the basic concept and recent results of the LASP, our seismic exploration package.

2. Lunar Active Seismic Profiler (LASP)

The LASP is a rover-transportable system with active sources and

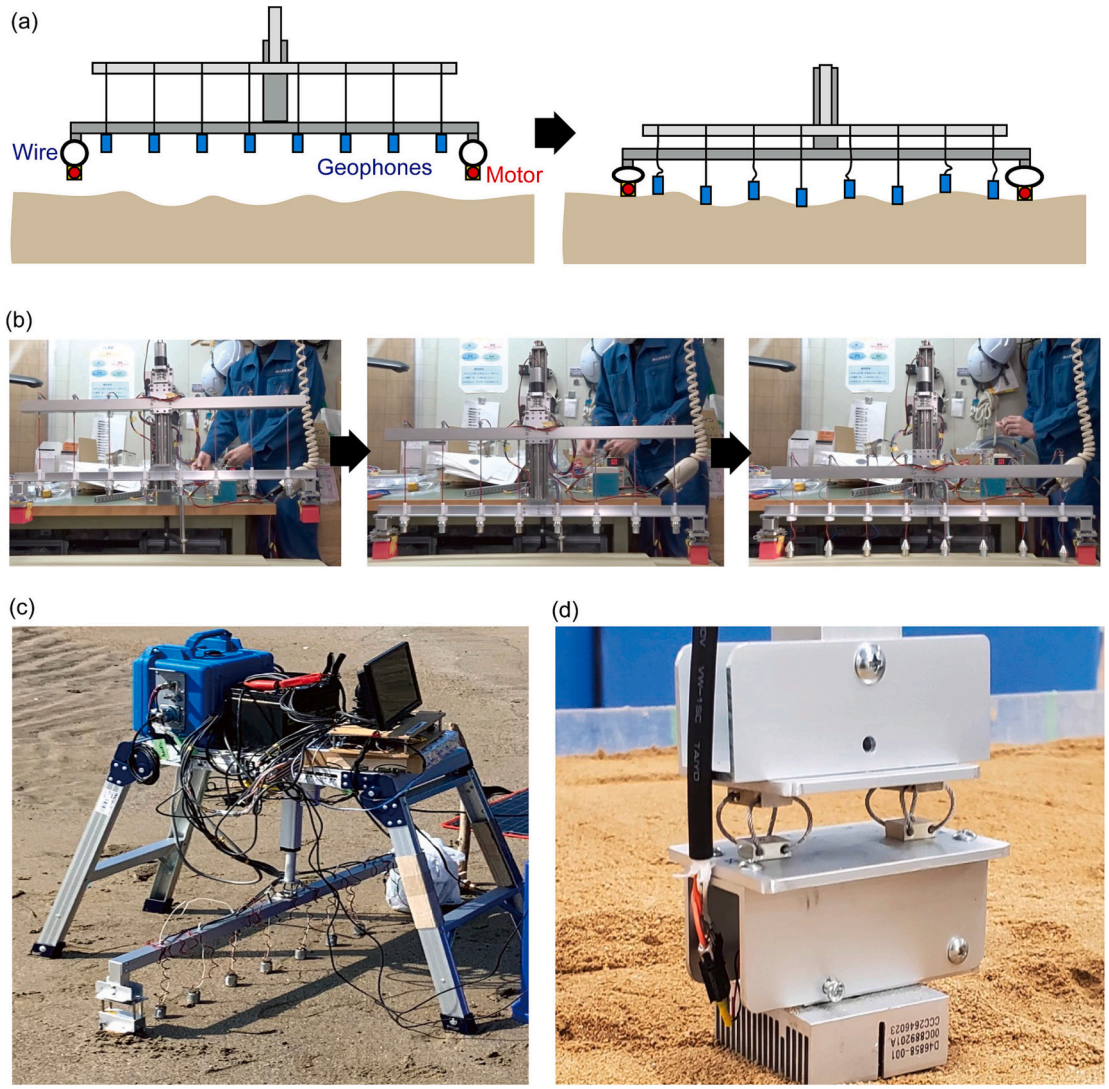

Fig. 1. Lunar Active Seismic Profiler (LASP). (a) Schematic diagram and (b) photos showing the operation of the LASP. (c) The LASP prototype during the field experiment (sand beach). (d) The portable active seismic source (PASS) deployed on the LASP. The wire cushion on top of the source provides a constant downward pressure and decreases the propagation of vibrations to the array frame.

multiple receivers on a minimal array <1 m long (Fig. 1). It is designed to obtain depth profiles of S-wave velocity between the ground surface and 1 m depth. The geophone array is deployed in a two-step process. First, a boom carrying all parts of the array is lowered, and seismic sources at each end are positioned on the ground surface. Then the geophones are lowered to the ground on thin strings that are threaded through the boom (Fig. 1a and b). We describe the key components of LASP (i.e., sources and receivers) below.

2.1. Seismic sources

Seismic sources for a portable array of this type can produce signals with a motor, a piezoelectric element, or the blows of a hammer. We conducted the experiments using all of these seismic sources. In this study, we show the results based on a motor-based source call the portable active seismic source (PASS) (Tsuji et al., 2023). In the source system, the motor generates a signal by rotating an eccentric mass upon an axis to generate a chirp waveform that ascends or descends in frequency between 20 and 250 Hz. The seismic source can be configured to generate a specific waveform. With the shallow depth of our target (~1 m), the higher frequencies range (e.g., 50–200 Hz) are appropriate for a surface wave analysis. These can be generated by a small motor <2 cm in diameter. Stacking the continuously generated waveforms can improve the signal-to-noise ratio of the resulting signal and make it possible to explore depths greater than conventionally possible. The previous study (Tsuji et al., 2023) confirmed that the signal from the seismic source with a 4 cm motor propagated to ~1 km when the signals were stacked 225 times. Although it may not be necessary to have such an extensive signal propagation (~1 km) for the short-offset LASP, we should consider such a source for longer-offset surveys, as discussed later.

To ensure good contact between the seismic source and the ground surface and to reduce internal noise, we used a cushion of curved wires to transfer the weight of the boom to the source motor while somewhat insulating the frame of the seismic array from the motor's vibrations (Fig. 1d). In our system, we deployed two source systems, one at each end of the array. If a rough surface geometry hampers good ground contact for one of two sources, we could obtain useful results with a single source. The size and shape of the source bottom attached to the ground surface should be optimized by considering conditions of the surface.

2.2. Receivers

Because our analysis ignores low-frequency signals (<5 Hz), we can use small receivers, such as geophones, which have become common in extraterrestrial applications. For example, the InSight mission deployed a small MEMS receiver on Mars (Knapmeyer-Endrun and Kawamura, 2020), and geophones will be deployed on Titan in DragonFly projects (Lorenz et al., 2021). Our LASP design typically uses an array of eight geophones (Fig. 1). Larger numbers of receivers increase the signal-to-noise ratio.

Geophones in our design are coupled to the ground by their own weight (~100 g for each). Our experiments have shown that geophones thus deployed produce stable dispersion curves that are similar to the results from buried geophones (see Section 4). The most important consideration is to prevent transmission of vibrations through the main array frame to the geophones. For this purpose, the geophones are suspended from the frame on thin strings, and once the geophones are seated the frame is lowered further to remove the tension of the strings and decouple the geophones from the array frame. This design also allows the geophones to be seated on irregular ground (Fig. 1a).

3. Surface wave analysis

We investigated the S-wave velocity of the shallow substrate through a surface wave analysis of the LASP data, a technique that has been widely used for near-surface characterizations (e.g., Foti et al., 2014; Socco et al., 2010; Ikeda et al., 2012) and to determine the distribution of buried ice (Tsuji et al., 2012b). We commonly used surface wave analysis for ambient noise, but this approach can be also used for the active source seismic data. We used multi-channel analysis of the surface wave (MASW; Park et al., 1999) to estimate dispersion curves from which the shallow S-wave velocity structure can be estimated. MASW is a robust approach to distinguish the fundamental mode of surface waves from higher modes, body waves, and other noises in the frequency–phase velocity (or wavenumber) domain. The method consists in placing the receiver array on a straight line with the active source and calculating the phase through a Fourier transform of the observed waveform. By applying surface wave inversion to dispersion curves, the S-wave velocity structure can be estimated by assuming a uniform horizontal structure beneath the array.

However, a simple application of MASW to the short-array LASP system often yields an unclear dispersion curve owing to noise in the signal. One reason may be transmission of vibrations from the array frame to the geophones that interferes with the desired signals transmitted through the ground. Another main reason is that heterogeneities around the ground surface, including topographic variation, complicate the task of extracting surface-wave signals and degrade the quality of the dispersion curves. To calculate dispersion curve from such low quality data, we applied time-frequency analysis using the continuous wavelet transform (CWT) technique. Kulesh et al. (2005) derived the spectral relation of surface waves in the wavelet domain, defined as the wavelet propagator, and Holschneider et al. (2005) described a process based on the wavelet propagator to extract surface-wave phase velocity, group velocity and attenuation coefficients from cross-correlations. Ikeda and Tsuji (2018) used the wavelet propagator to estimate phase velocity dispersion curves between two stations. Poggi et al. (2013) proposed a time-frequency-wavenumber analysis to estimate phase velocity dispersion curves from continuous recordings.

In this study, we improved the stability of phase velocity estimation by introducing the CWT approach into MASW (CWT-MASW; Ikeda and Tsuji, 2019). In this analysis, we first compute shot gathers from multichannel active-source data by applying cross-coherence analysis. We then stack the cross-coherence gathers from several shots at a single observation position. By applying CWT-MASW to the cross-coherence gathers, we estimate phase velocity dispersion curves. The CWT-MASW can be divided into two steps. In the first step, group velocity dispersion curves are estimated from stacked amplitude of shot gathers in time-group velocity domain with CWT. In the second step, phase velocity dispersion curves are estimated by MASW only using phase at arrival times of the group waves estimated in the first step. The second step allows us to give a large weight on localized surface wave signals if group velocities of surface waves are extracted in the first step.

4. Results and interpretation

4.1. Depth profile of S-wave velocity

We deployed the LASP on a site at a sand beach, where the poorly sorted sediment is a fair proxy of lunar regolith. To ensure optimal conditions, we conducted the experiment on the farthest part of the beach from the sea, where the sand is relatively less saturated with fluid. We generated chirp signals that combined up-sweep and down-sweep in frequency and recorded the waveforms with the receivers on the LASP. We identified clear surface waves on the cross-coherence gather (Fig. 2a). Because of short-offset data and limited frequency range of the source system, it was difficult to identify clear body wave on the cross-coherence gather. However, the experiments with longer offset data show clear body waves.

We applied the CWT-MASW approach for the surface wave to estimate stable dispersion curves (Fig. 2b), which we then inverted to obtain an S-wave velocity profile beneath the array (Fig. 2c). Because the

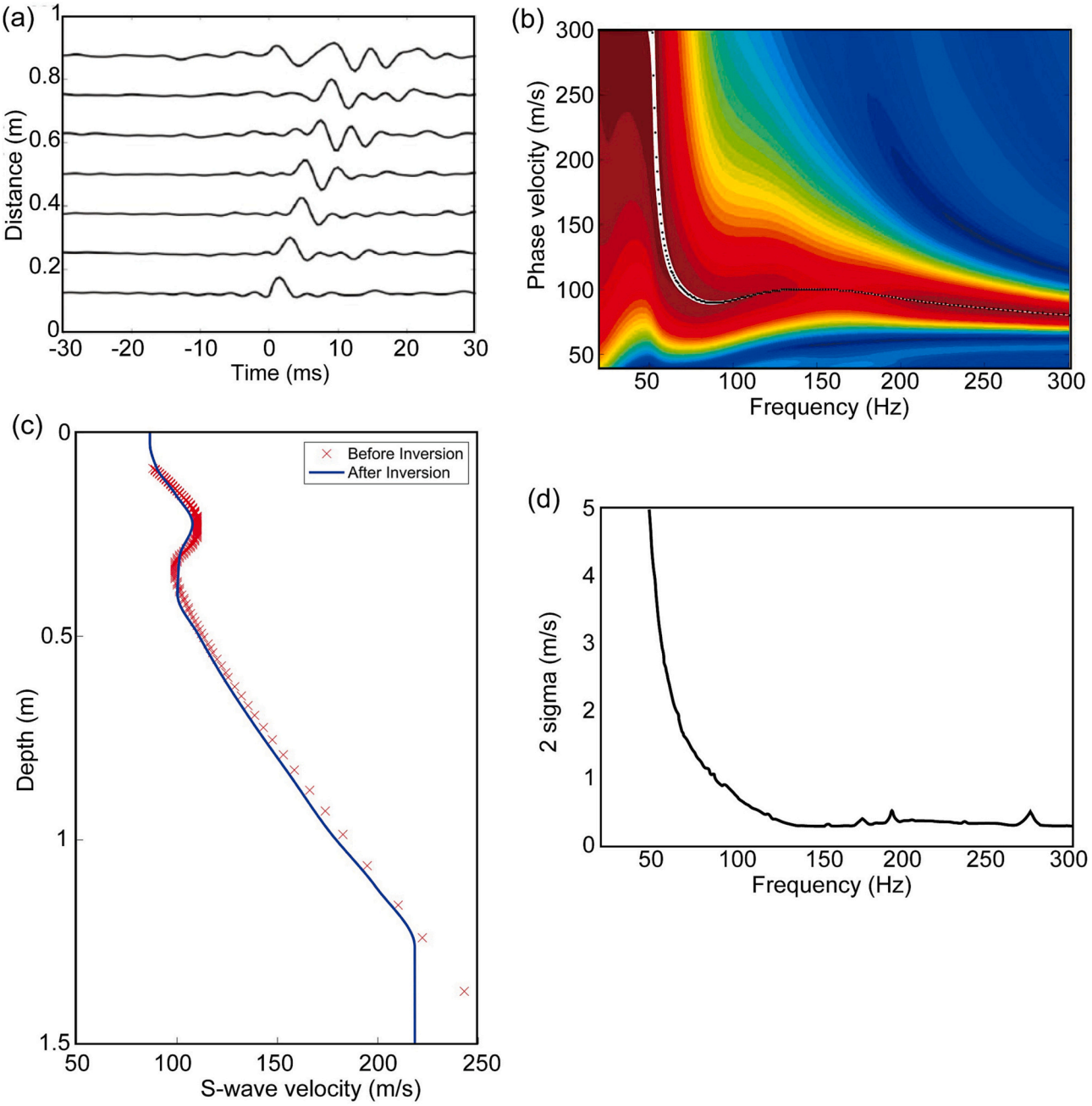

Fig. 2. Derivation of an S-wave velocity depth profile. This experiment was conducted at the sand beach shown in Fig. 1c. (a) Waveforms derived from cross-coherence analysis. The surface wave is clearly displayed on this gather. (b) Dispersion curve derived from the waveform in (a). The background color indicates the coherence. (c) The estimated S-wave velocity profile. Red crosses indicate the initial model, which was constructed from the dispersion curves in (b). (d) Two-sigma error as a function of frequency. (For interpretation of the references to color in this figure legend, the reader is referred to the web version of this article.)

velocity of the fundamental mode Rayleigh wave phase is sensitive to the S-wave velocity at depths around one-third of its corresponding wavelength, the dispersion curve can be converted to an approximate depth profile of S-wave velocity (red crosses in Fig. 2c). Using the S-wave velocity directly from the dispersion curve as initial model (red crosses in Fig. 2c), we estimated the depth profile of S-wave velocity via inversion (blue line in Fig. 2c).

To evaluate the accuracy of the estimated S-wave velocity, we calculated the error on the basis of 32 waveforms recorded at the measurement point, based on the bootstrap method (Efron and Tibshirani, 1993). We randomly selected waveforms from the 32 records to calculate the variance curve and repeated the same process 50 times to calculate the phase velocity uncertainty ($\pm 2\sigma$) from the 50 obtained dispersion curves. The results (Fig. 2d) indicate that the S-wave velocity was estimated with high accuracy (± 5 m/s).

4.2. *Equipment and analyses to improve dispersion curves*

We evaluated the dispersion curves under two different measurement conditions and two different analysis methods. In the laboratory, we compared the dispersion curves from two different deployment schemes, one involving buried geophones and the other involving geophones resting on the surface under their own weight (Fig. 3a). We conducted this evaluation using an artificial sand layer ~30 cm thick, which limited the frequency range of the dispersion curves because there was no sand layer deeper than 30 cm. The resulting dispersion

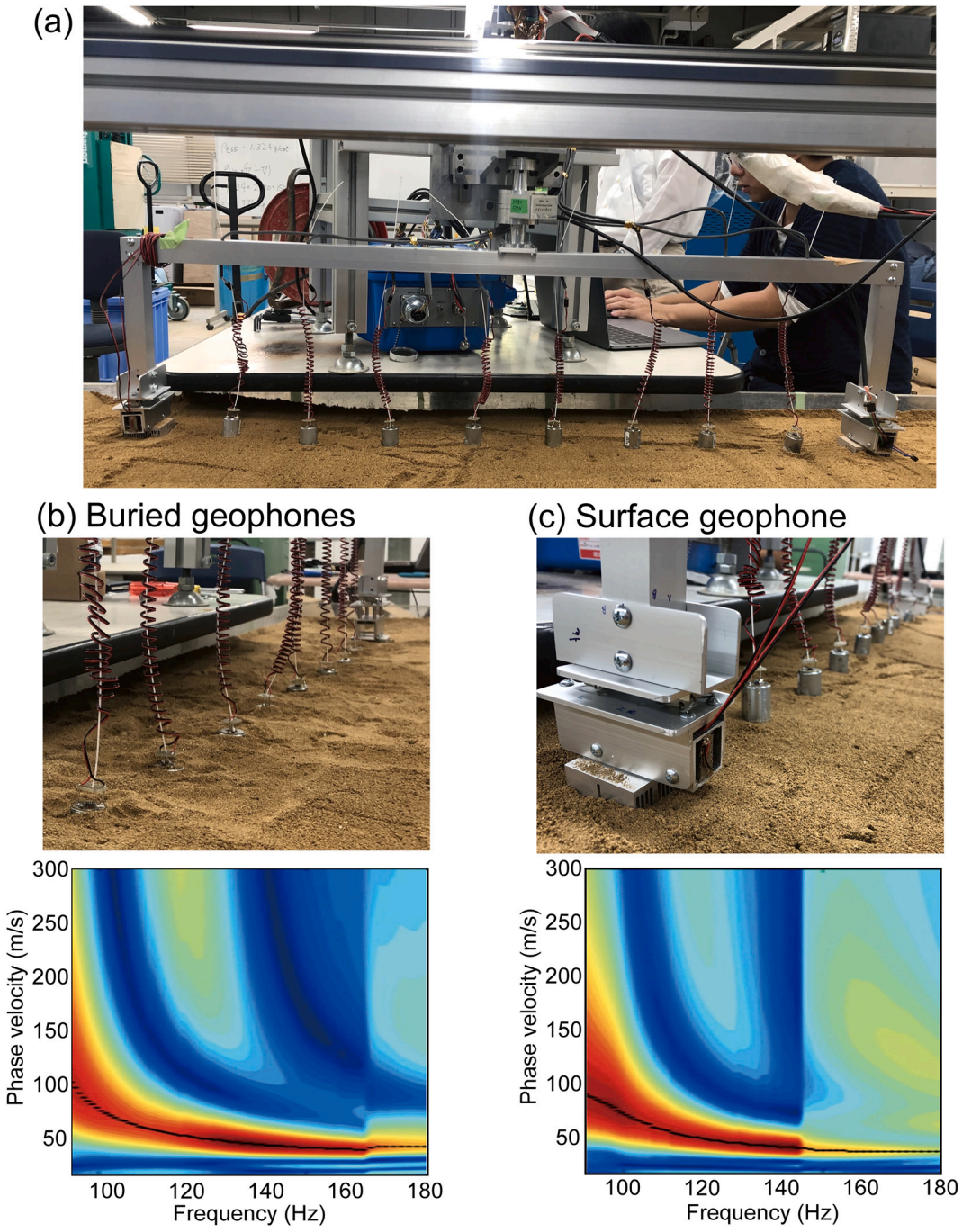

Fig. 3. Comparison of geophone placement. (a) Photo showing the LASP deployed in the laboratory experiment. (b) Photo and dispersion curve from a trial with buried geophones. (c) Photo and dispersion curve from a trial with geophones coupled to the surface by their own weight.

curves, derived using CWT-MASW, were similar (Fig. 3b and c). This result demonstrates that acceptable dispersion curves can be obtained by lightly coupled seismometers. Although we did not conduct the experiment in low-gravity conditions, our results suggest that placing geophones on the ground surface would be suitable for a deployment on the Moon, where ambient noise is very low and there is no wind. In the future work, it will be important to assess the geophone coupling in environments that closely resemble the lunar surface.

We also used this laboratory setup, with geophones placed on the ground surface, to compare the dispersion curves derived from conventional MASW and CWT-MASW analyses. The dispersion curve derived from conventional MASW was discontinuous (Fig. 4a) owing to scattering at the ground surface and vibration noise through the array frame. On the other hand, the dispersion curve from CWT-MASW was clean and stable (Fig. 4b), and we can expect to produce continuous dispersion curves on the Moon. Furthermore, previous studies (e.g., Onodera et al., 2022) have shown that scattering on the Moon is more dominant than on Earth. However, in our analysis of short-offset data, such scattering effects could not significantly influence the surface wave analysis.

4.3. *Three-dimensional S-wave velocity structure*

To obtain a 3D S-wave velocity structure, we obtained several intersecting seismic profiles in a prepared experimental plot measuring 6.5 m × 9 m containing a conical excavation (1 m deep and ~ 4 m wide)

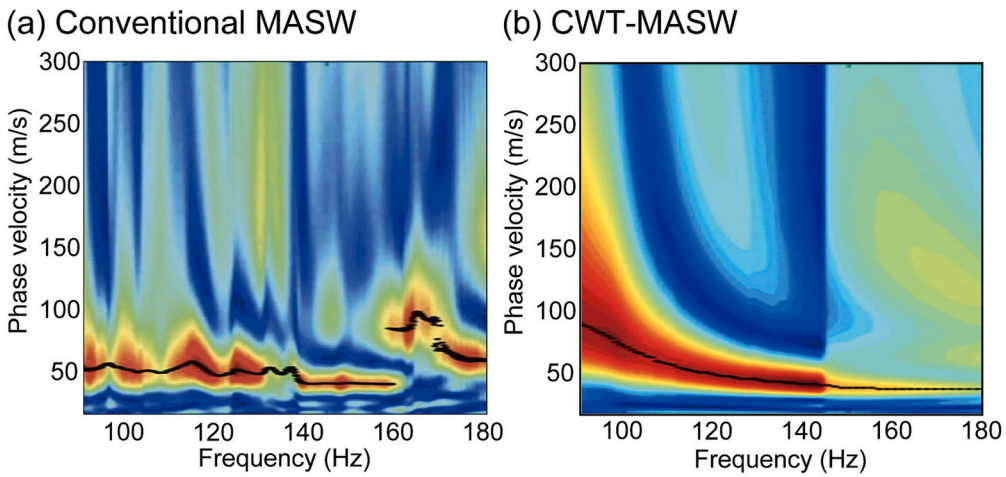

Fig. 4. Improvement of the dispersion curve by CWT-MASW. (a) Dispersion curve derived from conventional MASW. (b) Dispersion curve derived from CWT-MASW.

at its center that was filled with softer material; the whole field was then covered with 30 cm of softer material and compacted to different degrees with a heavy roller (Fig. 5). The shallow sediment along Lane A where the roller passed 2 times without vibration could be the softest (least compacted). On the other hand, Lane B where the roller passed 2 times with vibration could be the harder (more compacted) than Line A.

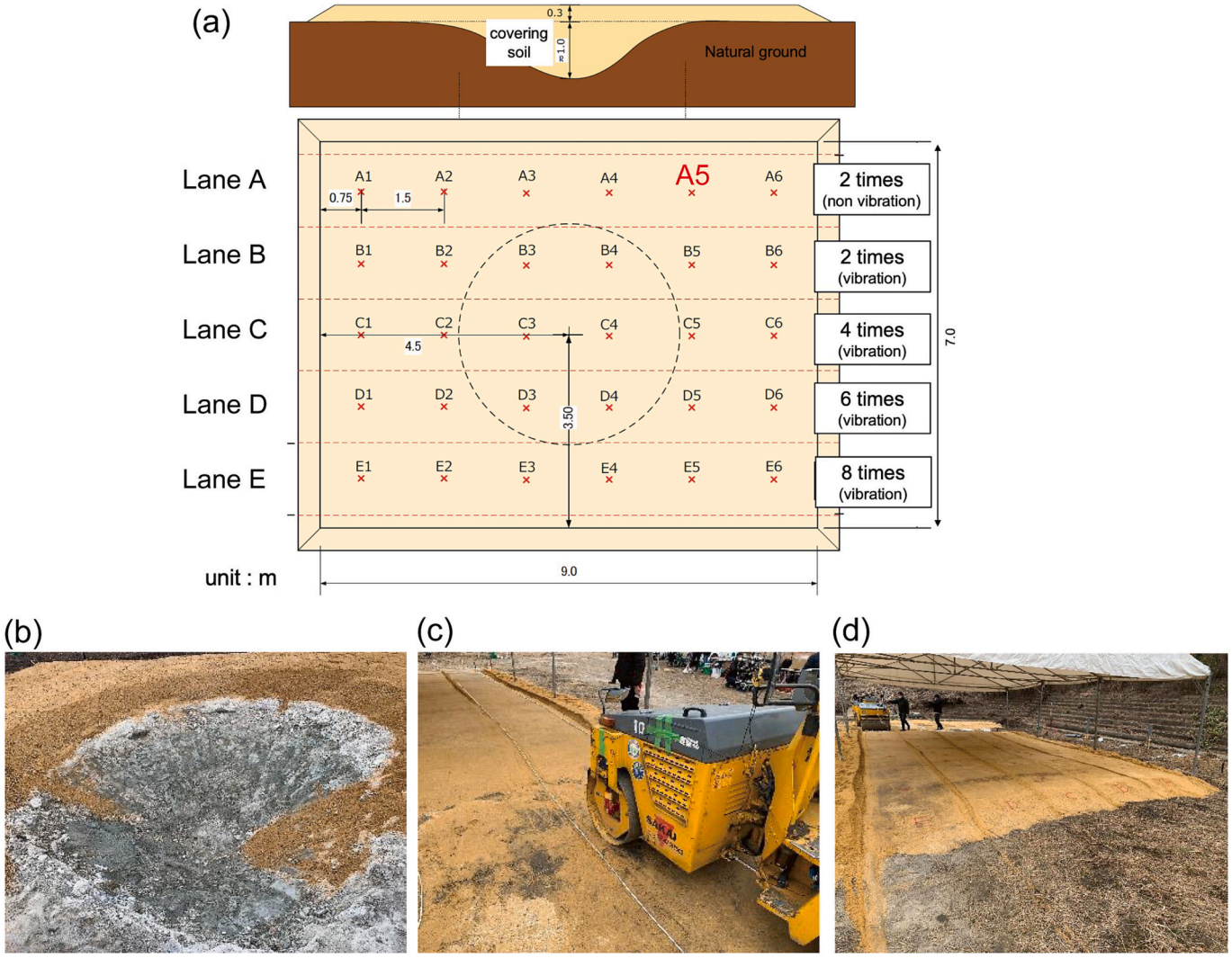

Fig. 5. Plan and photos of the test field. (a) Cross section and plan view of the field. The horizontal lanes were compacted by the passage of a motorized roller between two and eight times. In the upper line A, we did not vibrate the roller. But, in other lanes, we vibrated the roller to increase the stiffness. (b) The conical excavation before filling. (c) Roller compacting the field. (d) View of the fully prepared field.

Line E where roller passed 8 times with vibration could be the hardest (most compacted) in this test field (Fig. 5a). We measured S-wave velocity profiles at 30 positions and derived a 3D S-wave velocity model by interpolation. Note that we used motors of two different sizes; because the results were similar, we show only the results from the larger motor. Also, we separated the motors from the array system in this experiment because of the problem of the connection between seismic source and array frame (i.e., wire cushion) during this experiment.

Clear dispersion curves were obtained at most measurement positions in this experiment (Fig. 6a), partially because of the flat ground surface without topographic variation in the test field (Fig. 5c and d). Thus, we could estimate the dispersion curve and S-wave velocity through conventional MASW, without resorting to the CWT approach. The results demonstrate that the S-wave velocity ranged from 60 m/s near the surface to 260 m/s at depth (Fig. 7). The S-wave velocity of the shallow cover sediment was <120 m/s, a typical value for unsaturated shallow sediment. The buried concavity appeared as a low-velocity area at the appropriate depth (Fig. 7b and c). Furthermore, the different degrees of compaction were successfully detected as a gradient in S-wave velocities at 0.1 m depth between ~65 m/s and ~ 100 m/s (Fig. 7a); The S-wave velocity is low (65 m/s) without vibration of roller (Lane A in Fig. 7a), but S-wave velocity largely increases to 85 m/s by using vibration to increase the solid compaction (Lane B in Fig. 7a). Furthermore, similar S-wave velocity for Lanes D and E in our results (~100 m/s; Fig. 7a) demonstrates that roller compaction with >6 times does not largely increase the sediment compaction. The field experiment confirmed that we can detect spatial variations in compaction and lithology (e.g., depth of bedrock) with the LASP.

Because the array length of LASP (~1 m) is approximately equivalent to one wavelength of the surface wave utilized in our analysis, it is crucial to account for the near-offset effects that may influence phase velocity estimation (Roy and Jakka, 2017). These near-offset effects are attributable to several factors, such as body-wave contamination, and are related to subsurface structures and Vp/Vs ratio (e.g., Xu et al., 2006). However, previous studies (e.g., Aung and Leong, 2010; Yoon and Rix, 2009) demonstrated that phase velocity can be estimated at high frequency range even from near-offset data. The significance of near-offset effects should be carefully evaluated for the MASW analysis for the short source-receiver distance data. To evaluate the influence of near-offset effects on the dispersion curve in our field experiments (Figs. 5 and 7), we calculated the phase of the transfer function as a function of offset for each frequency (Fig. 6b). Considering the wavelength used in Fig. 6b, it is likely that the near-offset effects will be observed in the near-offset section of the receiver array (Park et al.,

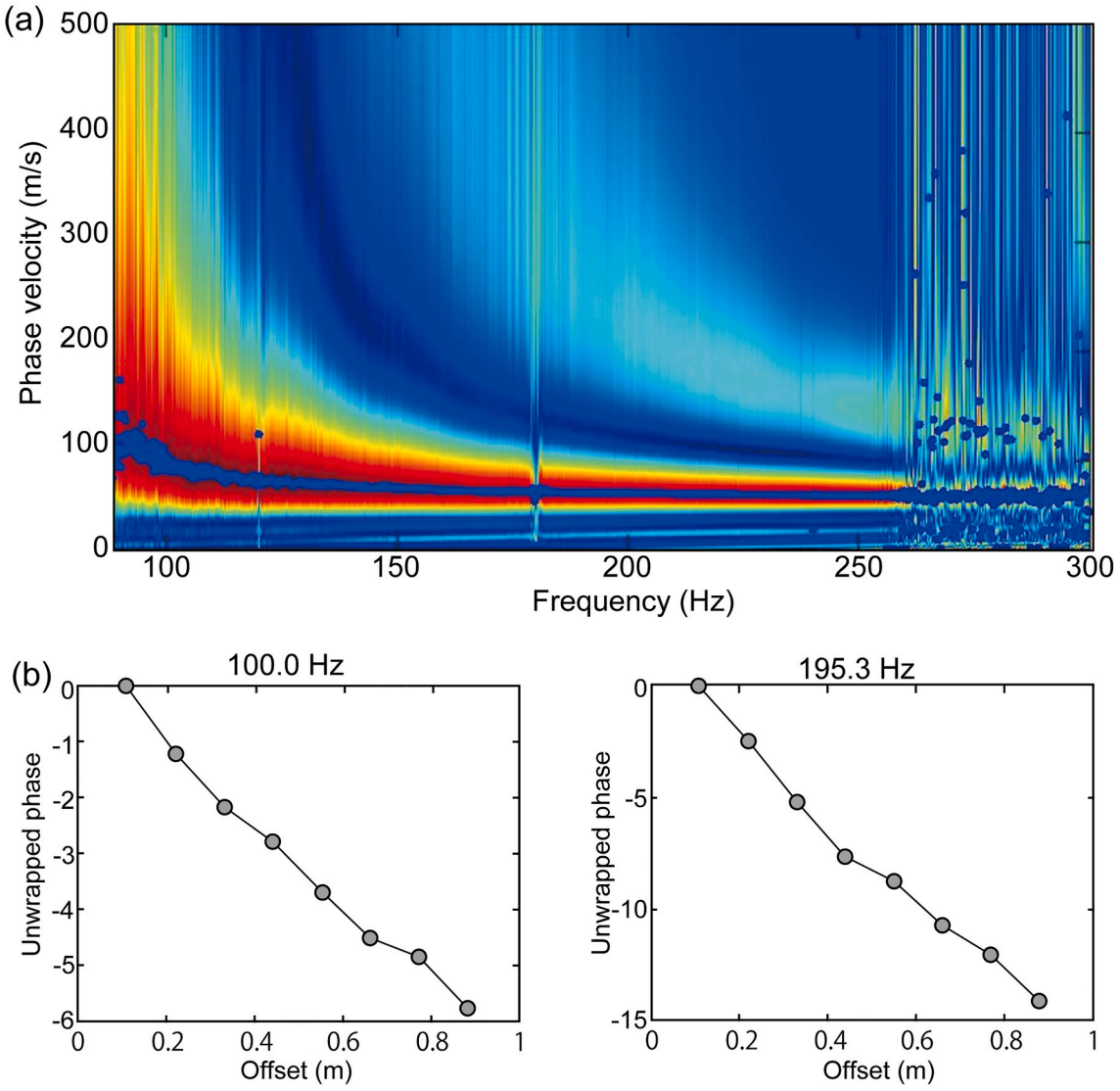

Fig. 6. Dispersion curve and phase of the transfer function at the test field. (a) Dispersion curve at position A5 in Fig. 5. (b) The relationships between phase of transfer function and offset at the position A5. Here we show the relationships for two frequencies.

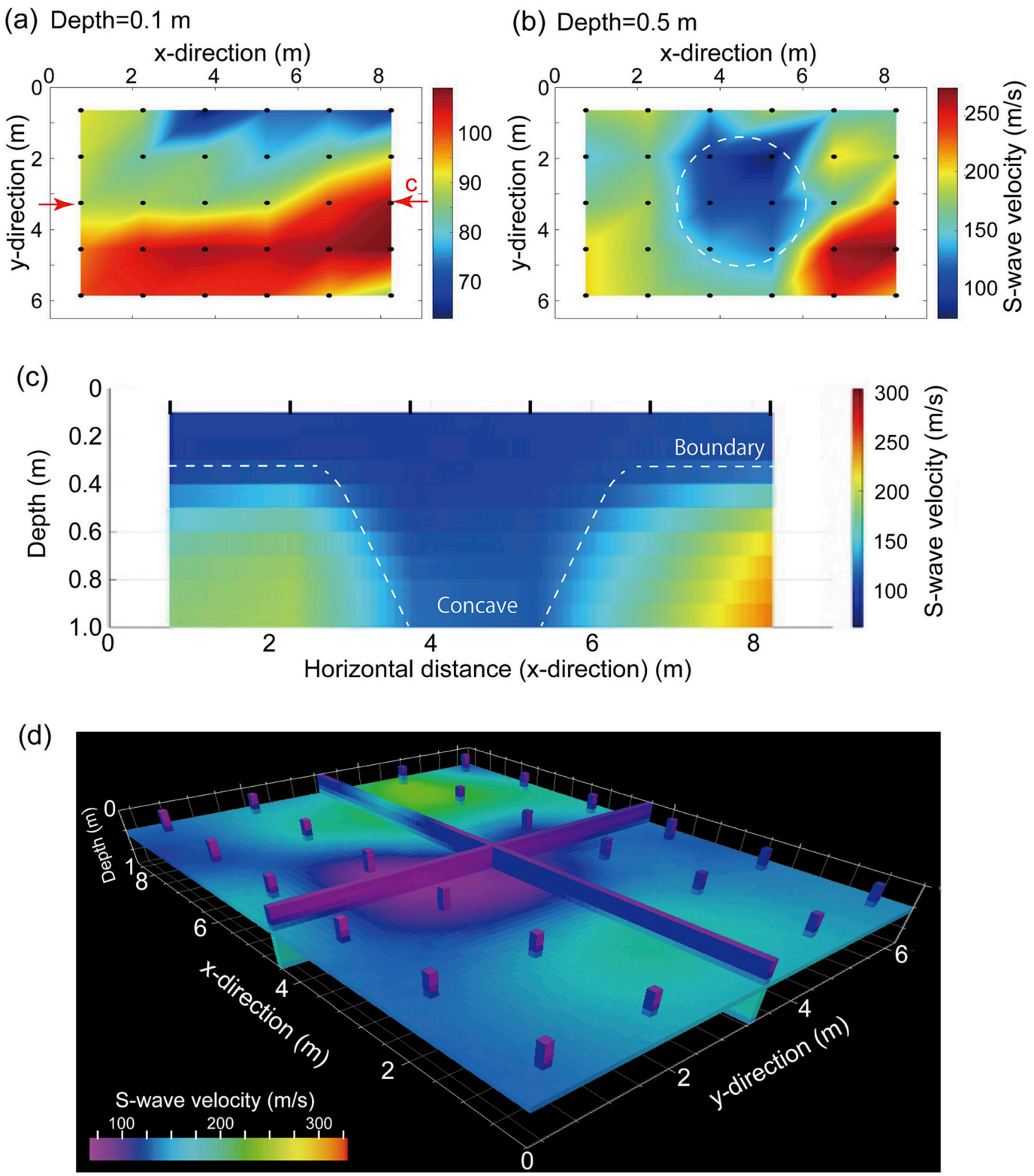

Fig. 7. Three-dimensional S-wave velocity model of the test field. (a) Depth slice (top view) of the S-wave velocity model at 0.1 m depth. (b) Depth slice at 0.5 m depth. Note the differing color scales in panels (a) and (b). (c) Depth profile across the center of the test field (see Fig. 5 for location of points). The white dashed line marks the lithological boundary between the geological substrate and the experimental cover sediment, including the conical excavation. (d) View of the estimated 3D S-wave velocity model obtained from 30 measurement points. Here we interpolated the S-wave velocity profiles using Kriging approach.

1999). However, the linear relationship between the phase and offset in Fig. 6b indicates that velocities estimated from near-offset section and far-offset section are same, suggesting that near-offset effects do not significantly impact our results. Additionally, the relationship between phase and offset depicted in Fig. 6b could prove useful in identifying receivers that produce inaccurate results (i.e., dispersion curve). If there is a receiver whose phase deviates significantly from the linear relationship between the phase and offset (Fig. 6b), excluding that receiver

from the analysis will result in a more stable dispersion curve.

5. Discussion and summary

Our results demonstrate that the LASP enables as to image the shallow subsurface with high accuracy (Fig. 2d). Our method is accurate enough to investigate the distribution of ice in extraterrestrial regolith. To evaluate the sensitivity of S-wave velocity for the freezing of ice, we conducted the laboratory experiment using regolith simulant (see Appendix). Because experiments show that S-wave velocity varies by ~40 m/s with the presence of 0.5 wt% ice (Fig. A2), the accuracy of velocities achievable with LASP data (~0.5 m/s in Fig. 2d) is good enough to identify regions with 0.5 wt% ice saturation as an S-wave velocity anomaly. Furthermore, with the LASP we can detect 3D subsurface structures, including lithological boundaries (Fig. 7). This information could be useful for construction of base camps as well as telescope deployments on the Moon. Furthermore, with LASP data we can map the degree of consolidation at shallow levels, information that is important for the design of rovers, including crewed rovers in future missions.

We have mainly focused on the application of our LASP for lunar exploration, but it could be used on other planetary bodies such as Mars, Titan, asteroids, and comets. For example, the DragonFly project will deploy multiple geophones in the legs of a drone (Barnes et al., 2021). Although the shape of the geophone array is not linear, a surface wave analysis can still yield good results by assuming a laterally uniform substrate beneath the seismic array. Furthermore, active seismic surveying as discussed here could be useful for the exploration of asteroids or comets, because passive seismic experiments in such environments could be difficult due to fewer quicks or less ambient noise. Our LASP experiments used eight geophones, but smaller numbers of geophones are also possible for a surface wave analysis. Indeed, a LASP unit with smaller number of geophones has been mounted on a drone and used to automatically conduct seismic experiments on Earth (Tsuji et al., 2021; Hamasato et al., 2023). The shallow seismic investigation method to identify small-scale anomalies have been recently required in many infrastructure projects on Earth (Tsoflias et al., 2006).

This study focused on the investigation of a shallow substrate (<1 m) based on surface waves. Because the length of the array (~1 m) is roughly consistent with the investigation depth of a surface wave analysis, our system cannot reach greater depths. Depths beyond 1 m require an array of commensurate dimensions. One way to achieve a long seismic array is to separate the seismic source and receiver by deploying them on different rovers. Because our seismic source generates repeated configurable signals (Tsuji et al., 2023), we can obtain long-offset data with two or more rovers that would obtain shot gathers at several shooting positions. Long-offset data would support seismic reflection or refraction analyses and yield 2D/3D seismic reflection profiles as well as 2D/3D P-wave velocity models in extraterrestrial environments. Furthermore, there are viable options with a single rover. A fixed seismic source could be placed near the lander while a rover with a geophone records the seismic signal from different positions and assembles a long-offset shot gather (Fig. 8a). This scheme would yield 3D S-wave velocity models based on surface wave analysis and 1D P-wave velocity profiles based on seismic refraction or reflection analyses. A similar approach has been used to produce a 3D S-wave velocity model in an extensive area of Earth (Ikeda et al., 2018). Conversely, the rover could carry the seismic source and the signal would be recorded by a geophone at a fixed position (Fig. 8b). The flexible geometry of seismic sources and receivers can make possible a wide range of extraterrestrial active seismic surveys.

Declaration of Competing Interest

The authors declare that they have no known competing financial

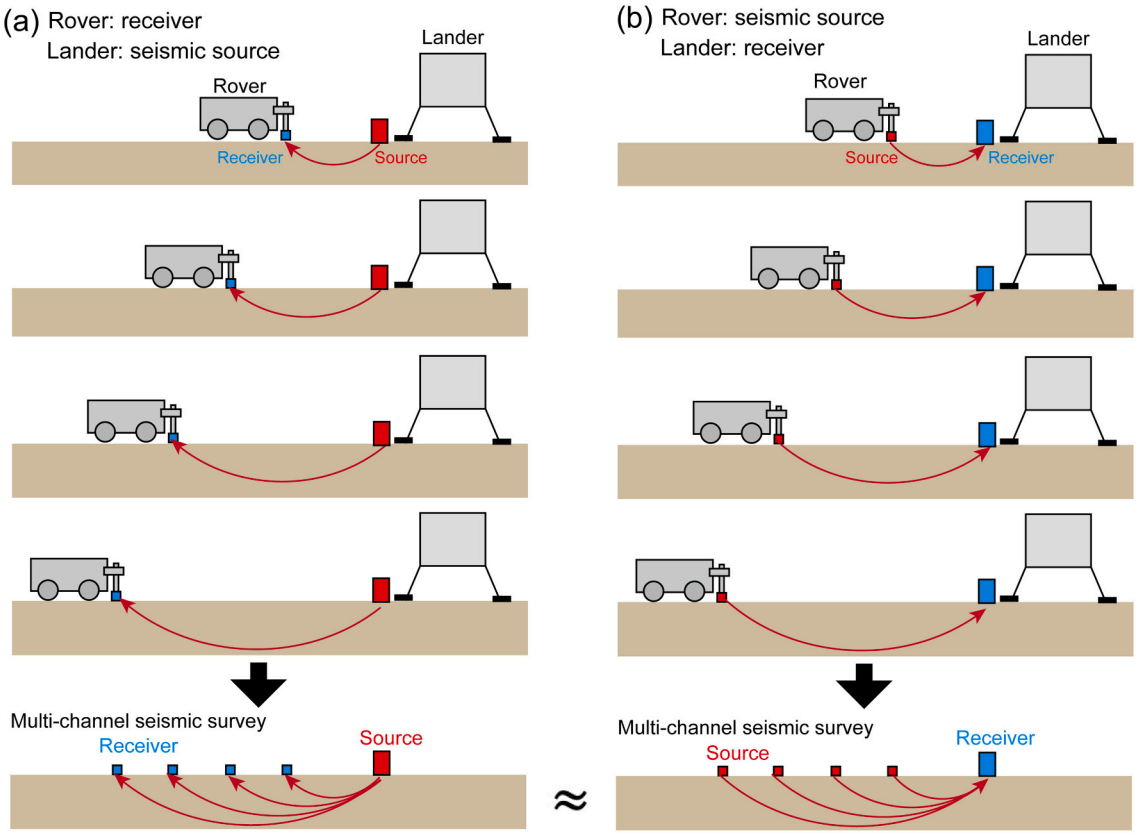

Fig. 8. Long-offset seismic surveys. (a) Fixed source and rover-mounted receiver. (b) Rover-mounted source and fixed receiver. Both approaches are effective in obtaining multichannel seismic data (bottom panels).

interests or personal relationships that could have appeared to influence the work reported in this paper.

Data availability

All data used in this paper were acquired in this study. The geophone data are available by communicating with the corresponding author.

Acknowledgements

This study was supported through the Japan Society for the Promotion of Science (KAKENHI grant JP20H01997; JP21H05202; JP22H05108), the Institute of Space and Astronautical Science/JAXA, and Project of technological innovation for Construction on Space field of the Ministry of Land, Infrastructure, Transport and Tourism. We thank Sean Gulick (UTIG) and another anonymous reviewer for constructive comments. We also thank K. Kitamura (Kyushu University) for providing the equipment for part of our seismic velocity measurements, and Yoshiaki Ishihara (JAXA) and Yuzuru Karouji (JAXA) for the fruitful discussion.

Appendix A. Relationship between S-wave velocity and ice saturation

One possible objective of a seismic survey is the estimation of ice saturation in the shallow substrate. We evaluated the effect of ice saturation on S-wave velocity in laboratory experiments that measured S-wave propagation in a simulated lunar regolith as it was cooled from room temperature to −18 °C inside a refrigerator and then returned to room temperature (Fig. A1). The dry regolith mixtures contained an added 0.1 wt%, 0.3 wt%, 0.5 wt %, 0.7 wt%, and 1 wt% of water, respectively. To obtain the samples for each saturation, we added certain amount of water mixed the certain amount of water and regolith simulant in the plastic bag.

We recorded 400 shots at intervals of 5 min, thus taking >33 h for each trial. The water was liquid at the start of each experiment, then turned to ice in the refrigerator, as shown by the change in waveforms (Fig. A2). After confirming that the water had frozen from the constant shape of waveforms, we took the sample from the refrigerator and allowed the ice to thaw. As the water froze, the S-waves propagated faster and the waveforms became constant. As the ice melted, the S-waves propagated slower, and the waveforms returned to their initial shape. The clear temporal variation indicates that the S-wave velocity was varied associated with freezing of water.

From the S-wave travel times, we calculated the S-wave velocity as a function of ice saturation (Fig. A2). Although the results at ~0.5 wt% ice saturation were not clear, the other trials showed that the S-wave velocity increased as a nearly linear function of ice saturation. From the results, we confirmed that a seismic survey would reveal an S-wave velocity anomaly of ~40 m/s that would detect 0.5 wt% ice saturation. We note that because S-wave velocity also depends on the distribution of ice in the pore space, the relationship between S-wave velocity and ice saturation could be influenced by the speed of freezing.

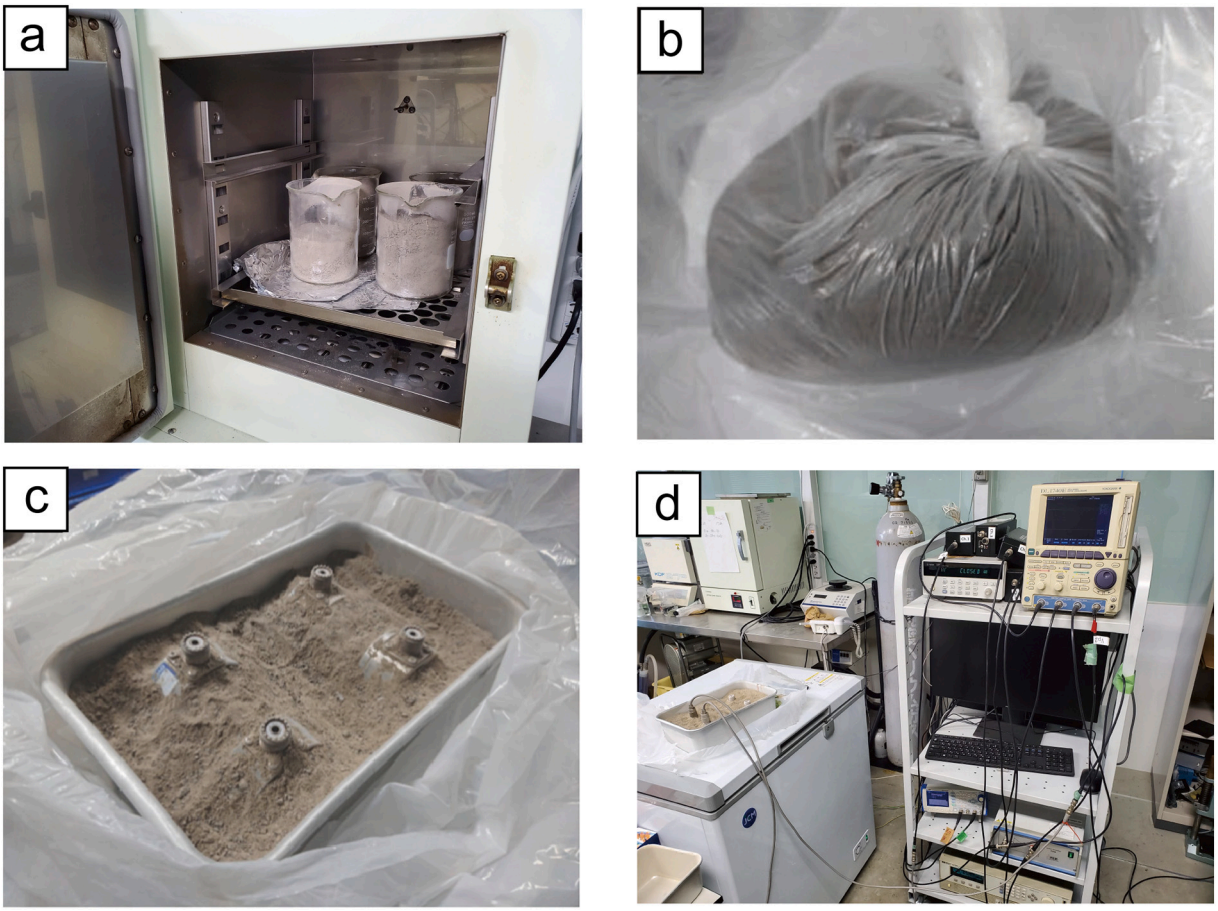

Fig. A1. Pictures of laboratory experiment. (a) Dry the lunar regolith simulant in oven. (b) Add certain amount of water mixed the certain amount of water and regolith simulant in the plastic bag. (c) Deploy the transducers of P-wave and S-wave within the regolith simulant. (d) The regolith simulant outside of the

refrigerator, and the equipment for seismic velocity measurement.

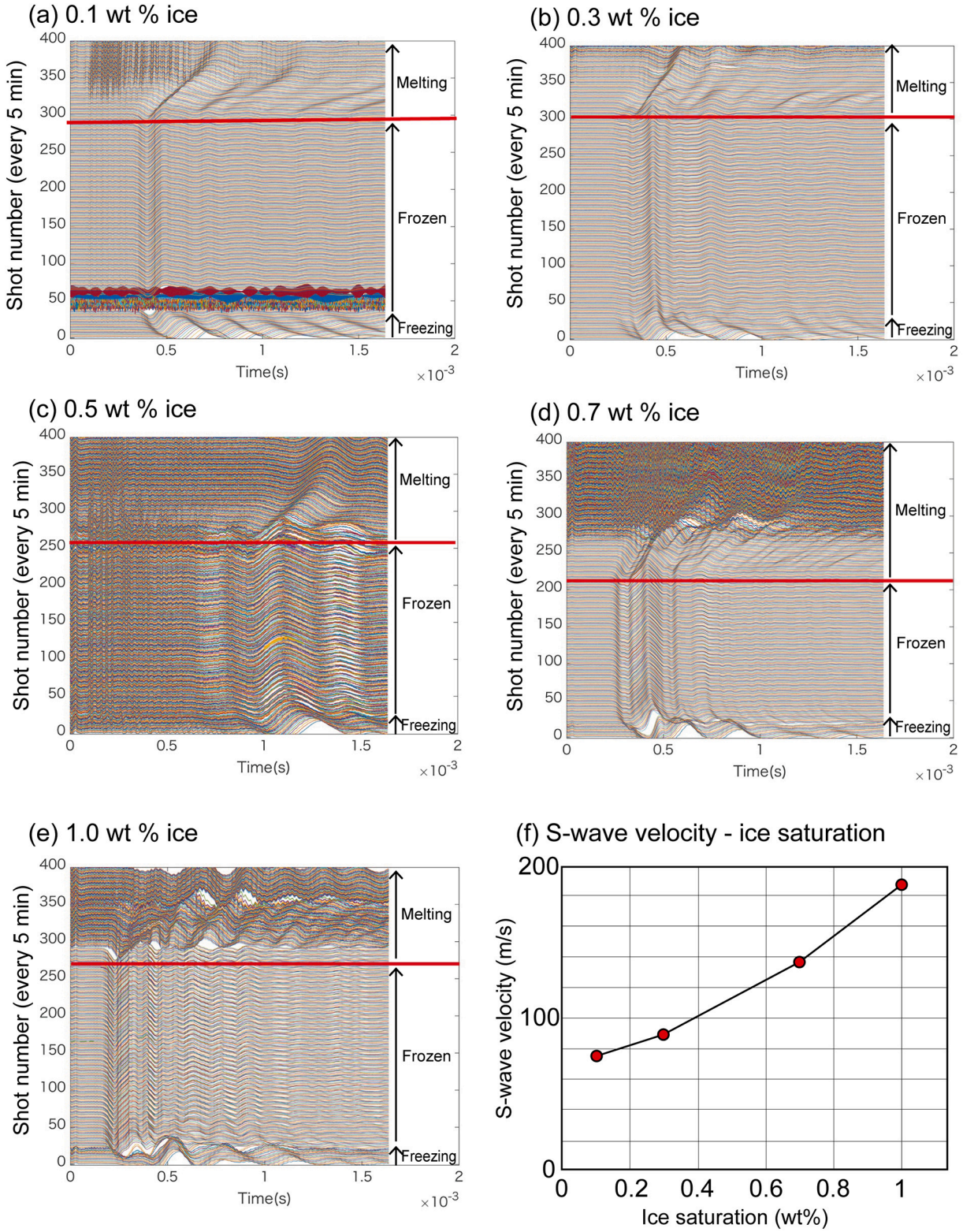

Fig. A2. S-wave velocity and ice saturation. (a–e) Temporal variation of recorded S-wave waveforms during freezing and thawing of dry sediment blended with (a) 0.1 wt%, (b) 0.3 wt%, (c) 0.5 wt%, (d) 0.7 wt% and (e) 1 wt% liquid water. Red lines indicate the time when the samples were removed from the refrigerator. (f) Relationship between S-wave velocity and ice saturation. (For interpretation of the references to color in this figure legend, the reader is referred to the web version of this article.)

References

Aung, A.M.W., Leong, E.C., 2010. Discussion of near-field effects on array-based surface wave methods with active sources by S. Yoon and G. J. Rix. J Geotechnol. Geoenviron. Eng. 136, 773–775.

Banerdt, W.B., et al., 2020. Initial results from the InSight mission on Mars. Nat. Geosci. 13, 183–189. https://doi.org/10.1038/s41561-020-0544-y.

Barnes, J.W., et al., 2021. Science goals and objectives for the dragonfly titan rotorcraft relocatable Lander. Planet. Sci. J. 2 (4) https://doi.org/10.3847/PSJ/abfdcf.

Brinkman, N., Schmelzbach, C., Sollberger, D., et al., 2022. In situ regolith seismic velocity measurement at the InSight landing site on Mars. J. Geophys. Res. Planets 127. https://doi.org/10.1029/2022JE007229 e2022JE007229.

Coorper, M.R., Kovach, R.L., Watkins, J.S., 1974. Lunar near-surface structure. Rev. Geophys. 12 (3), 291–308. https://doi.org/10.1029/RG012i003p00291.

Efron, B., Tibshirani, R., 1993. An Introduction to the Bootstrap, Monographs on Statistics and Applied Probability, Vol. xvi. Chapman and Hall, New York, 436 pp.

Foti, S., Lai, G., Rix, G., Strobbia, C., 2014. Surface Wave Methods for Near-Surface Site Characterization. CRC Press.

Hamasato, Y., Sakaguchi, A., Tsuji, T., Yamamoto, K., 2023. Drone-based surface-wave seismic survey optimization via a multiple traveling salesman problem. J. Robot. Mechatron. 35 (2), 271–278. https://doi.org/10.20965/jrm.2023.p0271.

Heffels, A., Knapmeyer, M., Oberst, J., Haase, I., 2017. Re-evaluation of Apollo 17 lunar seismic profiling experiment data. Planet. Space Sci. 135, 43–54. https://doi.org/10.1016/j.pss.2016.11.007.

Hobiger, M., Hallo, M., Schmelzbach, C., et al., 2021. The shallow structure of Mars at the InSight landing site from inversion of ambient vibrations. Nat. Commun. 12, 6756. https://doi.org/10.1038/s41467-021-26957-7.

Holschneider, M., Diallo, M.S., Kulesh, M., Ohrnberger, M., Lück, E., Scherbaum, F., 2005. Characterization of dispersive surface waves using continuous wavelet transforms. Geophys. J. Int. 163, 463–478.

Ikeda, T., Tsuji, T., 2018. Surface-wave tomography for near-surface characterization with continuous-wavelet transform for two-station crosscorrelation. SEG Techn. Prog. Exp. Abst. 2018, 2531–2535.

Ikeda, T., Tsuji, T., 2019. Multichannel analysis of surface waves with continuous wavelet transform for near surface applications. In: Fifth International Conference on Engineering Geophysics. https://doi.org/10.1190/iceg2019-012.1.

Ikeda, T., Matsuoka, T., Tsuji, T., Hayashi, K., 2012. Multimode inversion with amplitude response of surface waves in the spatial autocorrelation method. Geophys. J. Int. 190 (1), 541–552. https://doi.org/10.1111/j.1365-246X.2012.05496.x.

Ikeda, T., Tsuji, T., Nakatsukasa, M., Ban, H., Kato, A., Worth, K., White, D., Roberts, B., 2018. Imaging and monitoring of the shallow subsurface using spatially windowed surface-wave analysis with a single permanent seismic source. Geophysics 83 (6), EN23–EN38. https://doi.org/10.1190/geo2018-0084.1.

Johansen, T.A., Digranes, P., van Schaack, M., Lønne, I., 2003. Seismic mapping and modeling of near-surface sediments in polar areas. Geophysics 68, 566–573.

Kawamura, T., Grott, M., Garcia, R., 2022. An autonomous lunar geophysical experiment package (ALGEP) for future space mission. Exp. Astron. https://doi.org/10.1007/s10686-022-09857-6.

Kenda, B., et al., 2020. Subsurface structure at the InSight landing site from compliance measurements by seismic and meteorological experiments. J. Geophys. Res. Planets 125 (6) e2020JE006387, doi:10/1029/2020JE006387.

Knapmeyer-Endrun, B., Kawamura, T., 2020. NASA's InSight mission on Mars—first glimpses of the planet's interior from seismology. Nat. Commun. 11, 1451. https://doi.org/10.1038/s41467-020-15251-7.

Kovach, R.L., Watkins, J.S., Landers, T., 1971. Active Seismic Experiment, in Apollo 14 Preliminary Science Report NASA SP-272 163-174.

Kovach, R.L., Watkins, J.S., Talwani, P., 1972. Active Seismic Experiment, in Apollo 16 Preliminary Science Report NASA SP-315, Section 10.

Kulesh, M., Holschneider, M., Diallo, M.S., Xie, Q., Scherbaum, F., 2005. Modeling of wave dispersion using continuous wavelet transforms. Pure Appl. Geophys. 162, 843–855.

Lognonné, P., Banerdt, W.B., Pike, W.T., et al., 2020. Constraints on the shallow elastic and anelastic structure of Mars from InSight seismic data. Nat. Geosci. 13, 213–220. https://doi.org/10.1038/s41561-020-0536-y.

Lorenz, R.D., Shiraishi, H., Panning, M., Sotzen, K., 2021. Wind and surface roughness considerations for seismic instrumentation on a relocatable lander for Titan. Planet. Space Sci. 206, 105320 https://doi.org/10.1016/j.pss.2021.105320.

Onodera, K., Kawamura, T., Tanaka, S., Ishihara, Y., Maeda, T., 2022. Quantitative evaluation of the lunar seismic scattering and comparison between the Earth, Mars, and the Moon. J. Geophys. Res. 127 (12) https://doi.org/10.1029/2022JE007558 e2022JE007558.

Orita, M., Ikeda, T., Tsuji, T., 2021. Miniature seismometer array system for lunar underground structures investigation: evaluation of its exploration depth based on Apollo seismometer data. Butsuri-tansa 74, 79–91.

Park, C.B., Miller, R.D., Xia, J., 1999. Multichannel analysis of surface waves. Geophysics 64, 800–808.

Poggi, V., Fäh, D., Giardini, D., 2013. Time-frequency-wavenumber analysis of surface waves using the continuous wavelet transform. Pure Appl. Geophys. 170, 319–335.

Roy, N., Jakka, R.S., 2017. Near-field effects on site characterization using MASW technique. Soil Dyn. Earthquake Engi. 97, 289–303. https://doi.org/10.1016/j.soildyn.2017. 02.011.

Socco, L.V., Foti, S., Boiero, D., 2010. Surface-wave analysis for building near-surface velocity models — established approaches and new perspectives. Geophysics 75, 75A83–75A102.

Suemoto, Y., Ikeda, T., Tsuji, T., 2020. Temporal variation and frequency dependence of seismic ambient noise on Mars from polarization analysis. Geophys. Res. Lett. 47 (13) https://doi.org/10.1029/2020GL087123 e2020GL087123.

Tang, Z., et al., 2020. Physical and mechanical characteristics of lunar soil at the Chang'e–4 landing site. Geophys. Res. Lett. 47 (22) https://doi.org/10.1029/2020GL089499.

Tanimoto, T., Eitzel, M., Yano, T., 2008. The noise cross-correlation approach for Apollo 17 LSPE data: diurnal change in seismic parameters in shallow lunar crust. J. Geophys. Res. 113, E8. https://doi.org/10.1029/2007JE003016.

Tsoflias, G.P., Steeples, D.W., Czarnecki, G.P., Sloan, S.D., Eslick, R.C., 2006. Automatic deployment of a 2-D geophone array for efficient ultra-shallow seismic imaging. Geophys. Res. Lett. 33, L09301. https://doi.org/10.1029/2006GL025902.

Tsuji, T., Kobayashi, T., Aoki, S., Kanamori, H., Aizawa, T., Matsuoka, T., 2012a. Elastic properties of lunar regolith from vertical seismic profiling. In: Proc. 13th ASCE. https://doi.org/10.1061/9780784412190.010.

Tsuji, T., Johansen, T.A., Ruud, B.O., Ikeda, T., Matsuoka, T., 2012b. Surface-wave analysis for identifying unfrozen zones in subglacial sediments. Geophysics 77, EN17-EN27.

Tsuji, T., Kawamura, T., Araya, A., Nagata, Y., Ishihara, Y., Ogawa, K., Kobayashi, T., Tanaka, S., Aizawa, T., 2019. Lunar Active Seismic Profiler (LASP): investigation of shallow regolith layer for resource exploration and base camp construction. SEG Glob. Meet. Abstr. 11-14 https://doi.org/10.1190/SEGJ2018-004.1.

Tsuji, T., Kinoshita, J., Tsuji, S., Yamamoto, K., Ikeda, T., 2021. Drone-based active source multichannel seismic survey system. In: Summit on Drone Geophysics, 30 pp., available at. https://seg.org/Portals/0/OpenContent/Files/9503/2021_Summit_on_Drone_Geophysics_-_Program_Booklet.pdf (last accessed Feb 2023).

Tsuji, T., Tsuji, S., Kinoshita, J., Ikeda, T., Ahmad, A.B., 2023. 4 cm Portable Active Seismic Source (PASS) for meter- to kilometer-scale imaging and monitoring of subsurface structures. Seismol. Res. Lett. 94 (1), 149–158. https://doi.org/10.1785/0220220049.

Xu, Y., Xia, J., Miller, R.D., 2006. Quantitative estimation of minimum offset for multichannel surface-wave survey with actively exciting source. J. Appl. Geophys. 59 (2), 117–125. https://doi.org/10.1016/j.jappgeo.2005.08.002.

Yoon, S., Rix, G.J., 2009. Near-field effects on array-based surface wave methods with active sources. J. Geotech. Geoenviron. Eng. 135, 399–406.

Zimmermann, R.W., King, M., 1986. The effect of the extent of freezing on seismic velocities in unconsolidated permafrost. Geophysics 51, 1285–1290.